Available online at www.sciencedirect.com
SCIENCE DIRECT®
Agricultural and Forest Meteorology 132 (2005) 96–114
AGRICULTURAL AND FOREST METEOROLOGY
www.elsevier.com/locate/agrformet

Assessment of automatic gap fraction estimation of forests from digital hemispherical photography

Inge Jonckheere [a,*], Kris Nackaerts [b], Bart Muys [a], Pol Coppin [a]

[a] *Katholieke Universiteit Leuven, Laboratory for Forest, Nature and Landscape Research, Vital Decosterstraat 102, 3000 Leuven, Belgium*

[b] *Intergraph Mapping and Geospatial Solutions, Intergraph Benelux (Belgium) B.V. (NASDAQ: INGR), Tennessee House, Riverside Business Park, Internationalelaan/Bld International, 55 B5, 1070 Brussels, Belgium*

Received 7 December 2004; accepted 6 June 2005

Abstract

Thresholding is a central part of the analysis of hemispherical images in terms of gap fraction and leaf area index (LAI), and the selection of optimal thresholds has remained a challenge over decades. The need for an objective, automatic, operator-independent thresholding method has long been of interest to scientists using hemispherical photography. This manuscript deals with the comparison of a wide variety of different well-known automatic thresholding techniques against the subjective manual method, using high-dynamic range digital hemispherical photographs. The performance of the different thresholding methods was evaluated based on: (1) visual inspection by means of a multi-criteria decision system and (2) quantitative analysis of the methods' sensitivity to an overall performance criterium. The automatic Ridler clustering method proved to be the most robust thresholding method for various canopy structure conditions. This automatic method might be the best solution for a fast, reliable and objective use of hemispherical photographs for gap fraction and LAI estimation in forest stands, given that the threshold setting is no longer manually performed. The fine-tuning potential of local thresholding methods to better address particular photographic limitations (e.g. over-exposure in a certain image region) is also presented.

Keywords: Gap fraction; Hemispherical photography; LAI; Thresholding

1. Introduction

1.1. Hemispherical photography

In ecological, hydrological, geo-morphological and biophysical process modelling, the forest canopy is generally characterized by leaf area index (LAI), defined as the total leaf area per unit ground surface area (Watson, 1947). LAI is the most common and,

* Corresponding author. Tel.: +32 16 329770; fax: +32 16 329760.
E-mail address: Inge.Jonckheere@biw.kuleuven.be (I. Jonckheere).

0168-1923/$ – see front matter © 2005 Elsevier B.V. All rights reserved.
doi:10.1016/j.agrformet.2005.06.003

Nomenclature

L_e	effective LAI
m_b	sample mean of gray values associated with background (sky) pixels
m_f	sample mean of gray values associated with foreground (vegetation) pixels
P	zenith angle in the hemispherical object region
P'	distance from the centre of the image
P_s	number of image pixels classified as sky
P_{ns}	number of image pixels classified as vegetation
r	radial distance
R	radius of hemispherical photograph
T	threshold value
$T(\theta, \alpha)$	gap fraction for a range of zenith angles with mean angle θ and angular resolution α
α	angular resolution
θ	zenith angle

arguably, most useful comparative measure of vegetation structure in forest canopies. This is especially critical when considering that the forest canopy is the functional interface between 90% of Earth's terrestrial biomass and the atmosphere (Ozanne et al., 2003). Rapid, reliable and accurate measurements of forest LAI are of fundamental importance to estimate the exchange of carbon, water, nutrients and light in numerous studies on the Earth's ecosystems.

The usefulness of indirect LAI determination in forest monitoring by means of hemispherical photography has already been demonstrated (see review of indirect methods in Jonckheere et al., 2004). Digital hemispherical photography analysis provides a valuable alternative for the accurate quantification of canopy structure, since canopy structure parameters (such as canopy cover and gap fraction) can be extracted from the photograph. LAI subsequently can be determined from gap fraction measurements by inverting a light interception model. However, the first step in such an analysis is the segmentation of hemispherical photographs in order to identify the gap fraction (or the complementary canopy cover). Consistent extraction of gap fraction (GF) from color hemispherical photographs is still one of the main technical challenges in the processing of data from this optical imagery. Accurate segmentation is of the utmost importance, given that the outcome of this step will have significant influence on all subsequent processing.

Hemispherical canopy photography traditionally has relied upon analog black and white or color films, and CCD-scanners to produce digital images for analysis (Fraser, 1997). The use of traditional analog hemispherical photography for GF and LAI determination not only leads to time-consuming analysis, but its limited 6-bit dynamic range (i.e. maximum 64 discrete brightness levels) also cause problems (Hinz et al., 2001). This low dynamic range causes difficulties in distinguishing sunlit leaves from relatively small, under-exposed gaps in the canopy. A leaf illuminated by direct sunlight might, for example, is not distinguishable from the surrounding sky, since the brightness difference is too small to be detected by the imaging system. Camera exposure settings therefore have a major impact on the GF and LAI measurements and are a major cause of measurement errors as demonstrated by Chen et al. (1991).

Commercial consumer-priced digital cameras offer a dynamic range of 8 bits (256 levels, e.g. Nikon Coolpix 950, Nikon, Japan), with a spatial resolution close to that of film emulsions (Hale and Edwards, 2002). These characteristics provide forest scientists with a practical alternative to traditional film photography (Frazer et al., 2001). The dynamic range of professional digital sensors nowadays ranges between 12 and 16 bits (4096–65,536 levels, e.g. Kodak DCS series, Eastman Kodak, USA). The resolution of camera sensors, equipped with high-resolution detector arrays (six million pixels and more) is fast becoming comparable to traditional 35 mm and larger film cameras (Russ, 2002). Consequently, modern digital image enhancement technologies offer remarkable opportunities to improve hemispherical canopy image quality and contrast.

Jonckheere et al. (2004) presents a detailed discussion related to analog and digital hemispherical photography, and the practical and technical advantages of digital hemispherical photography.

The quality of the fisheye optics is a constraint in the cases of both digital hemispherical and analogue photography. In essence, hemispherical photographs produce a hemisphere of directions on a plane (Rich,

1990), while the exact nature of the projection varies according to the lens used. The simplest and most common hemispherical lens geometry is the polar or equi-angular projection (Frazer et al., 1997), which assumes that the zenith angle θ of an object in the sky is directly proportional to the distance along a radial axis within the image plane. In a perfect equi-angular projection with a 180° field of view, the resulting circular image shows a complete view of all sky directions, with the zenith in the centre of the image and the horizons at the edges.

Accurate measurements of canopy gap size depend entirely on the projection of the image. Herbert (1986) has suggested that even small amounts of uncorrected angular distortion might cause substantial error in the measurement of gap area and distribution. As every lens invariably exhibits a (small) deviation from the theoretical projection, a lens correction should be applied to correct for view angle and angular lens distortion of the fisheye converter. The lens correction function can be calculated, which describes the expected angle position in an equal angle projection as a function of the actual observed angle of a full-resolution digital image. A third-order polynomial is sufficient for such corrections in the case of GF determination (Frazer et al., 2001). Fitting the polynomial to the lens correction function forces the polynomial to pass through zero and the maximum angle of the lens.

1.2. Thresholding and gap fraction extraction

One of the main problems cited in the processing of hemispherical photography is image segmentation, and thresholding, in particular. Thresholding corresponds to the selection of the optimal brightness value as threshold in order to distinguish vegetation from sky components, therefore producing a binary image from color photographs (Blennow, 1995; Jonckheere et al., 2004). A series of commercial software packages/freeware for processing hemispherical 1–24-bit imagery have been developed in the past and were used in a broad range of applications: WinSCANOPY (Regent Instruments, Qué., Canada, Rich et al., 1993), SOLARCALC (e.g. Ackerly and Bazzaz, 1995), Winphot (ter Steege, 1997), HemiView (Delta-T Device, Cambridge, UK, e.g. Battaglia et al., 2002), Gap Light Analyzer (GLA) (Frazer et al., 1997; Rhoads et al., 2004) and CIMES (Walter et al., 2003). However, most of these software packages are based on the interactive (manual) application of a visually selected threshold for the whole image, which has proven to be a source of inconsistency and/or error, with variations dependent on the observers' subjectivity (Englund et al., 2000). Interactive thresholding also is too time-consuming to apply to large numbers of images, and is consequently not appropriate for a robust, autonomous thresholding system (Koller et al., 1994). Jonckheere et al. (2004) formulated the need for a more efficient and robust classification technique and stated that automatisation of the thresholding was a requirement for moving towards an efficient and consistent post-processing effort of hemispherical photographs.

Previous research has also demonstrated that with high-dynamic range color imagery (36-bit and higher bit ranges, red–green–blue (RGB)), the choice of the threshold level would be less critical when compared to lower dynamic range devices. This is due to the frequency reduction of mixed pixels in higher resolution cameras, compared to the aggregation of pixels in cameras with lower resolution (Blennow, 1995; Nackaerts et al., 1999b). A high-dynamic range digital camera, therefore, would have the potential to improve the separability between vegetation and sky elements (Nackaerts et al., 1999a; Jonckheere et al., 2004). Another advantage related to high-resolution imagery is that various combinations of techniques may be applied to any one or all of the three RGB arrays, which might reduce the uncertainty associated with the green fraction that is often significant for forest canopies (Fernandes et al., 2003).

The scope of this paper, therefore, is to focus on the *gap fraction extraction* step in the process of calculating LAI from high-dynamic range (36-bit) hemispherical photographs. The research deals with influencing factors and methods in this image-processing step. A sensitivity analysis was performed based on digital 36-bit RGB images. The effects of operator bias and image thresholding methods were investigated.

Although optical devices are often used to estimate LAI, we chose to report gap fraction, which is the basic measurement of these instruments. LAI is quantitatively derived from the gap fraction and a model of leaf angle distribution, but since the

Table 1
Characteristics of the forest test sites in Belgium

Location	Brugge	Roeselare	Sint-Joris-Weert	Hechtel-Eksel	Hoeilaart
Forest site	Sterre forest	Tillegem forest	Meerdaal	Pijnven	Zoniën
Coordinates	50°55′N 3°08′E	51°10′N 3°11′E	50°48′N 0°20′E	51°10′ N 5°19′ E	50°47′ N 04°26′ E
Average site elevation (m)	25	10	75	55	110
Date of acquisitions	13 August 2001	14 August 2001	6 March 2002	7 October 2002	10 October 2003
Weather conditions	Blue sky	Blue sky	Cloudy	Cloudy	Cloudy
Cover type	Deciduous	Coniferous	Coniferous	Coniferous	Deciduous
Species composition	*Fagus sylvatica* L.	*Pseudotsuga menziesii* (Mirbel) Franco and *Larix decidua* Mill.	*Pinus nigra* subsp. *laricio* Maire	*Pinus sylvestris* L.	*Fagus sylvatica* L.
Maximum canopy height (m)	20	35	20	25	30

inversion of gap fraction to LAI is another pressing issue in indirect optical LAI determination, this last step in LAI determination was not considered as part of the scope of this paper. There is not yet a consensus in literature concerning gap fraction-LAI inversion with questions related particularly to (1) the choice of light interception model to use for the description of leaf angle distribution in forests and (2) the correction factors to apply for conversion of optical effective LAI (L_e) estimates to LAI (Chen, 1996). Different light interception models were used by various authors, e.g. Chason et al. (1991), Oker-Blom and Kellomäki (1983), Oker-Blom et al. (1991) and Mussche et al. (2001). Discussions related to correction for clumping and the effect this has on the conversion of effective LAI to LAI is partially described in Stenberg et al. (2003) and Weiss et al. (2004).

2. Materials and methods

2.1. Kodak DCS 660 technology for gap fraction assessment

2.1.1. Study sites

An extensive dataset of over 300 hemispherical photographs was collected between August 2001 and October 2003 from five forests stands in Belgium. Gap fraction and LAI measurements also have been monitored intensively for this stands, thereby allowing comparison of results. All sites were relatively homogenous stands, and most were measured with various optical devices, such as LAI-2000 (Licor Inc., NE, USA) and TRAC Instrument (3rd Wave Engineering, Ont., Canada) during field inventories and LAI measurements (Jonckheere et al., 2005). The sites include two deciduous and three conifer stands in Belgium with a variety of canopy structures (open/closed). Canopies were selected at all sites to prevent a high under-story layer that may influence the indirect optical measurements. Relevant information concerning the stands can be found in Table 1.

2.1.2. Camera characteristics

The Kodak DCS 660 used in this study is a digital professional camera, consisting of a Nikon body and lens, and a Kodak digital back plane. The heart of the system is a 6.2 mega pixels (3040 × 2008 pixels) charge-coupled-device (CCD) array. The aperture and shutter priority both were set manually, and digital RGB images were stored on an internal PCMCIA-ATA hard disk in 36-bit (12-bit/color) format. Images were downloaded directly from the digital camera to the computer for further analyses.

2.1.3. Image acquisition

The camera and lens were attached to a self-leveling mount (Delta-T Device, Cambridge, UK), which was oriented by corner pins on a tripod. This set-up ensured a consistent level positioning of the camera during image acquisitions. The top of the lens was 1.3 m above the ground and the camera was oriented such that the magnetic north was always located at the top of the photographs. Photographs were taken during conditions of diffuse skylight (blue sky or evenly overcast), with normal exposure settings in the evening time when

the sun was under the skyline in order to minimize glare from direct sunlight. Photographic images were recorded using a Sigma 8 mm f/4 'fisheye' lens (Sigma Corporation, Tokyo, Japan) at the highest possible resolution (3040 × 2008 pixels) with highest ISO setting (ISO 200). Moreover, the focus ring was set to infinity when using the fisheye lens, as depth of field is practically infinite and focusing was not required (Bockaert, 2004).

2.2. Data processing

2.2.1. Pre-processing of the images

The color hemispherical photographs were analysed using the ENVI (2004) image-processing software package for Windows (RSI, Version 4.0, CO, USA). As absorption of leafy material is maximal and scattering of sky tends to be lowest in the blue channel, the blue channel was chosen for subsequent analysis based on previous research on low dynamic range imagery. This highlighted maximal contrast between leaf and sky and the compatibility with the LAI-2000 that measures light intensities solely below 490 nm (Jacquemoud and Baret, 1990; Nackaerts et al., 1999b). However, the smallest vegetation elements might be invisible in the blue channel, especially during blue sky conditions. This is due to the limited quality of the hemispherical lens, which suffers chromatic aberration, especially in the blue part of the spectrum (Frazer et al., 2001). These outcomes resulted in a trade-off effect between the two counteracting factors when using the blue band for GF analysis.

Kucharik et al. (1997), however, claimed that the use of all three bands, instead of only one channel, allows for the incorporation of optical characteristics in the discrimination between vegetation elements and sky. This statement was investigated by analyzing own data before processing of the imagery. The blue channel and circular image was extracted from the RGB image by means of an in-house developed PHP script (PHP, 2004) and based on two programming libraries for 16-bit images: ImageMagick and Xite (ImageMagick, 2004; Xite, 2004). The products were visually compared to the multispectral version of the photograph in ENVI (Version 4.0, RSI, CO, USA).

The blue channel turned out to be the best single RGB channel for the discrimination between sky and vegetation, a result that is in agreement with that found by Nackaerts et al. (1999b). However, when the blue channel was compared to the RGB image, the use of all three bands resulted in more discernable detail in sunlit image areas (Fig. 1). In this study, the full spectral resolution (three bands), subsequently was used in further imagery processing, given that the use of three bands was technically feasible and no compatibility was required with other optical devices.

2.2.2. Lens calibration

A procedure for calibrating the view angle and lens distortion of the fisheye lens was developed based on unpublished data provided by Sigma Corporation

Fig. 1. RGB analysis vs. blue channel.

(Tokyo, Japan). The data consisted of 23 specifications with regard to the actual relationship between radial distance r and zenith angle θ. A lens correction function was calculated based on calibration data to correct for deviations from the equi-angular projection. This was done in order to minimize aberrations due to the high sensitivity of gap fraction analysis to angular distortion. The relationship between radial distance r and zenith angle θ was fitted by means of the statistical software of Table Curve 2D (Version 4.0, Systat, London, UK) to a polynomial expression of the form:

$$P' = \sum_{i=0}^{N} a_i P^i \quad (1)$$

where i is the order of the term, N the order of the polynomial expression, P' the distance from the centre of the image (in mm) and P is the zenith angle θ in the hemispherical object region. By changing the order of the polynomial expression from unity to 20, the change in the standard error estimate (SEE) with the order N was analyzed (Zar, 1984). The expression with minimum SEE was determined as the optimum expression for calibrating the view angle and lens distortion of the Sigma fisheye converter. The standard error of polynomial correction expression decreased significantly from the first- to third-order of term from 0.25 to 0.0192. No more decrease in standard error was shown after the third-order of term. Consequently, the third-order polynomial expression was determined as the optimum expression for calibrating view angle and lens distortion because of the minimum SEE (0.0192). The numerical coefficients were: $a_0 = -0.0009$, $a_1 = 0.1367$, $a_2 = -0.0000154$ and $a_3 = -0.00000155$, respectively. This polynomial expression was used to correct the view angle and lens distortions by substituting the radial distance at a given point r and the radius of hemispherical photograph R into the obtained polynomial expression in ENVI.

Two more steps were required to derive gap fraction from the digital RGB images: (1) the separation of pixel intensities into sky and vegetation classes by thresholding and (2) the calculation of gap fraction.

2.2.3. Thresholding

Thresholding is the simplest and most fundamental segmentation method. In a gray level image, for example, a gray value would be chosen such that pixels with intensities below or equal to the treshold would represent one class (e.g. feature), whereas those above the threshold would represent the other (e.g. background). This technique is used to transform a color image into a black and white image. Thresholding is an effective tool to separate vegetation from sky, given that the gray levels of pixels representing vegetation in hemispherical photographs are substantially different from the gray levels of pixels belonging to the sky background (Otsu, 1979; Sezgin and Sankur, 2004). The output of the thresholding operation is a binary image whose foreground represents vegetation and can be assigned a gray level of 0 (black), whereas the background corresponds to the sky and can be represented by a gray level of 65,535 in 16-bit (white). Gap fraction can then easily be extracted as the ratio of sky pixels to the total amount of pixels in the image, given this binary image as input.

The shape of the gray scale histogram often facilitates manual selection of the threshold value, for example, with the mid-point or a valley between two distinct peaks often used as threshold (Prewitt and Mendelsohn, 1966). Unfortunately, this method is undesirable for two reasons. First, the nature of the image histogram may be uni- or multi-modal such that the selection of the appropriate value is less obvious. The threshold selection is unrepeatable under these circumstances, due to the inherent subjectivity in the decision-making process and inter-operator variation. Secondly, manual thresholding, apart from being extremely impractical for image acquisitions dealing with large numbers of images, can be complicated by various factors, such as noise, ambient illumination and inadequate contrast (Lievers and Pilkey, 2004).

The commonly used but subjective manual thresholding will consequently be tested against automatic methods for image binarization in this study.

For the manual thresholding, the image processing software ENVI was used to allow the full dynamic range (16 bits) of the images, thereby avoiding the conversion of the data to a lower bit range and the concomitant reduction in quality. Other commercial available software packages for gap fraction and LAI estimation could not be applied, as they are all limited to 8-bit image processing. An experienced operator selected for each image individually the best visual

threshold in order to discriminate foliage from the sky background. All pixels with brightness values higher than the threshold are than classified as sky, whereas all pixels lower than the threshold are foliage.

Concerning the automatic methods, however, selecting an appropriate one can be a difficult task since there are many automatic thresholding algorithms published in literature. The caveat is that different algorithms typically produce different results, since they make different assumptions about the image content. For instance, some require the two classes to be dissimilar in size, while others model the class distribution as normals, etc. (Rosin and Ioannidis, 2003). The selection of segmentation algorithms in this study was based on algorithms that are widely known and straightforward to implement, thereby ensuring that accurate coding was likely.

The selected automatic methods can be categorized in six groups, according to the information they require (see the overview by Sezgin and Sankur (2004) for a description of the individual methods):

(1) *Histogram shape-based methods*: this category of methods achieves thresholding based on the shape properties of the histogram. Analysis is based on the histogram of the luminance values in the image (peaks, valleys, etc.). The tested methods in this groups were the method of Rosenfeld, Sezan, Olivo and Ramesh (e.g. Olivo, 1994).
(2) *Clustering-based thresholding methods*: in this class of algorithms, the gray level data undergoes a clustering analysis, with the number of clusters set always to two. The gray levels are clustered in two classes as background and foreground. Examined methods were Ridler, Yanni, Otsu, Lloyd, Kittler and Jawahar (e.g. Ridler and Calvard, 1978).
(3) *Entropy-based methods*: this class exploits the entropy of the distribution of gray levels in an image. The maximization of the entropy of the thresholded image is interpreted as indicative of maximum information transfer. Some algorithms use the entropy of the foreground and background regions, while others focus on the cross-entropy between the original and binarized image, etc. Methods of Kapur, Sahoo, Pun, Li, Brink and Shanbag were investigated (e.g. Kapur et al., 1985).
(4) *Object attribute-based methods:* these algorithms select the threshold value based on some attribute quality or similarity measure between the original image and the binarized version of the image. These attributes can be, for example, edge matching, connectivity, texture, shape compactness, etc. The Tsai method, Hertz, OGorman, Huang and Pikaz method were used (e.g. Tsai, 1985).
(5) *Spatial methods*: this class utilizes not only gray value distribution but also dependency of pixels in a neighbourhood, for example, in the form of correlation functions, 2D entropy, co-occurrence probabilities and local linear dependence models. High-order probability distribution and/or correlation between pixels are then used for segmentation. The method of Pal, Abutaleb and Beghdadi were tested (e.g. Abutaleb, 1989).
(6) *Local methods*: in this class of algorithms, a threshold is calculated at each pixel, which depends on some local statistics, such as range, variance, etc. The threshold value is adapted to the local image characteristics of the neighbourhood. The method of Niblack, Sauvola, White, Bernsen, Palumbo, Kamel, and Yanowitz was tested as representative of this group (e.g. Niblack, 1986).

The different categories tested in this study and their main characteristics and threshold determination are shown in Table 2. Further details regarding each algorithm are provided in the respective references and in the overview of Sezgin and Sankur (2004).

Image segmentation, and thresholding in particular, is a body of research that is important in fields as diverse as document analysis, medical imaging and computer vision. While many different thresholding algorithms have been proposed, the appropriate selection is application-dependent. The automatic methods tested in this study consequently are widely used in the field of microscopy and medicine, but only few of them were used and/or investigated to optimise thresholding in hemispherical canopy photography. For example, Weiss (2003) used the convex-hull thresholding method (as histogram shape-base thresholding) in EYE-CAN Version 1.4 and Nackaerts et al. (1999a) used the Cluster–Otsu method combined with the local Niblack method to correct for light errors in 24-bit photographs. In most studies and

Table 2
Overview of tested thresholding method categories

Category	Threshold T based on	Reference
Histogram shape-based	Shape (e.g. valley after the first peak) properties of histogram	e.g. Olivo (1994)
Clustering-based	Midpoint between two clusters by iteratively estimating the mean of two cluster means	e.g. Ridler and Calvard (1978)
Entropy-based	Consideration thresholding image as two classes of events with each class characterized by a probability function (pdf). T is converging point by maximizing the sum of the entropy of the two pdf	e.g. Kapur et al. (1985)
Object attribute-based	Attribute quality or similarity (e.g. texture) of input image preserved in the output image	e.g. Tsai (1985)
Spatial	Gray value distribution and dependency of pixels in a neighbourhood	e.g. Abutaleb (1989)
Local methods	Calculation of T (i, j) at each pixel of the coordinates (i, j) which depends on some local statistics like mean, range, variance, etc. of the pixel neighbourhood (of size b × b)	e.g. Niblack (1986)

software used for processing hemispherical imagery, however, a threshold is usually applied interactively, which leaves plenty of space for operator differences and inconsistency. To our knowledge, no survey exists that has focused on an extensive study concerning automatic thresholding for gap fraction and LAI estimation.

Fifty digital photographs, 10 for each of the 5 forest sites, were randomly selected from the photographic database of over 300 images in order to study thresholding algorithm performance. Thirty-five different automatic methods were tested against the operator-based manual method, where a (global) threshold was visually selected for each image in the image-processing program ENVI by an operator. The visual analysis was evaluated by means of a multi-criteria decision system, based on the performance of the algorithm in two situations: (1) to detect sunlit foliage as vegetation and (2) to detect small gaps at the edges which appear darker than sky pixels in the centre of the image. In addition to visual inspection, the results were quantified using the method of Sezgin and Sankur (2004) for evaluation of the thresholding algorithms. The thresholded images were evaluated visually with ENVI and quantitatively by means of an overall average thresholding performance score (AVE). AVE was calculated by averaging the normalized scores of five performance criteria by means of a module in Otimec, an image analysis software (Sezgin and Sankur, 2004). The five performance criteria were: (1) misclassification error (ME), (2) region non-uniformity (NU), (3) edge mismatch (EMM), (4) relative foreground error (RAE) and (5) modified Hausdorff distance (MHD). The different criteria are presented in Table 3, with performance measures varying from 0 for an absolutely correct segmentation to 1 for a totally erroneous case (Sezgin and Sankur, 2004, Table 3).

Table 3
Overview of thresholding performance criteria (Sezgin and Sankur, 2004)

Performance criteria	Explanation
Misclassification error (ME)	Percentage of background pixels wrongly assigned to foreground, and conversely, foreground pixels wrongly assigned to background
Region non-uniformity (NU)	Ratio of the foreground variance in the thresholded image to the variance of the whole thresholded image
Edge mismatch (EMM)	Discrepancies between the edge map of the gray level image and the edge map obtained from the thresholded image
Relative foreground area error (RAE)	Comparison of area properties of the objects, as obtained from the segmented image with respect to the reference image
Modified Hausdorff distance (MHD)	Parameter to asses shape similarity of the thresholded regions to the ground-truth shapes
Arithmetic average performance score of image (AVE (i))	Arithmetic mean of ME, NU, EMM, RAE, MHD calculated for image (i)

A single thresholding method that results in perfect agreement with the standard reference image is unlikely, given the methods of thresholding described above. Nevertheless, there will always be a thresholding method that will yield the closest possible agreement results, being most robust in terms of both visual and quantitative analysis. We refer to this as the ''optimal'' thresholding method. This technique will be further evaluated in the sensitivity analysis.

2.2.4. Gap fraction estimation

The last step in the interpretation of the classified hemispherical photographs in terms of gap fraction is the calculation of the gap fraction from the binary black-and-white images. Gap fraction, defined as the fraction of open sky not obstructed by canopy elements, can easily be calculated for different zenith and azimuth angles. This is done by counting the amount of sky pixels and vegetation pixels by means of the following formula:

$$T(\theta, \alpha) = \frac{P_s}{P_s + P_{ns}} \quad (2)$$

where $T(\theta, \alpha)$ is the gap fraction for a range of zenith angles with mean angle θ and angular resolution α; P_s is the number of pixels classified as ''sky pixels'' in a region centred at (θ, α) and P_{ns} is the number of vegetation pixels within a region centred at (θ, α). GF was computed after calibrating the view angle and lens distortions of the Sigma fisheye lens. All photograph processing were fully automatized by means of an in-house developed IDL (2004) script to extract gap fraction (IDL, Version 6.1, RSI, USA), resulting in no interference by an operator. The comparison between the different digital photographs in the sensitivity analysis, where the effect of threshold and operator bias was examined, was done at the resulting gap fraction level to gain a good understanding of the influencing factors.

3. Results

In this section we present the results obtained by following the testing protocol of both visual inspection and the quantitative performance analysis.

3.1. Visual analysis

The results of the visual analysis of 50 photographs thresholded by the different thresholding algorithms are listed in Table 4. Apart from algorithm performance in the centre of the image (to detect sunlit foliage as vegetation) and at the edges (to pick up small gaps which appear darker than the sky pixels in the centre of the image), the overall visual appearance (artificial patterns) of the image also was investigated (Table 4).

Worst and best case images, based on visual inspection for each of the six investigated thresholding method categories, are given in Fig. 3. These are shown along with the reference ground-truth images and the manually thresholded image.

At first glance, the results in Table 4 showed that most of the algorithms performed better under bright conditions than in dark regions. The histogram shape-based and local thresholding algorithms generally were too sensitive to overall image differences in gray levels in the hemispherical canopy photographs. Fig. 3j illustrates this problem. Small differences in gray levels between stems and background vegetation, for example, caused the Sezan algorithm to select a threshold value in-between, thereby classifying slightly brighter background vegetation as sky. Fig. 3a and b illustrate the local white and Niblack methods, which were even more sensitive and resulted in extremely noisy images. The method of Rosenfeld, also a local thresholding method was not sensitive enough, and many vegetation pixels were lost by this technique (Fig. 2c). It shows that at the edge of the image and on areas with a closer canopy, small gaps in the canopy were strongly exaggerated. Some of the entropy, attribute-based and local algorithms (e.g. Pikaz, Bernsen) performed well in the centre of the image, but tended to classify too many pixels as vegetation at the edges, which yielded too dark results (Fig. 3c and d).

Other methods, for example, shape Olivo and entropy Shanbag, were not sensitive enough and many vegetation pixels were lost by these techniques (Fig. 3e and f). Some methods exhibited artifacts after thresholding, for example, the object attribute-based OGorman method and the local Yasuda method, which resulted in angular and abrupt edges (Fig. 3g and h). Algorithms that performed best in visual terms were the clustering method of Ridler, the attribute-based method of Hertz, and the spatial method of

Table 4
Performance evaluation of 35 automatic thresholding methods, based on visual inspection of a random selection of 50 RGB hemispherical canopy photographs, taken under different canopy structure conditions and camera settings

	Category	Subcategory	Methods	Visual evaluation		
				Center and sunfleck performance	Edges and under-exposured regions	Overall appearance
Manual				Fair results	Fair results	±
Automatic	Histogram shape-based	Convex hull	Rosenfeld	Too few details	Too few details	−
		Peak and valley	Sezan	Too few details	Too few details	−
			Olivo	Too few details	Too few details	−
		Shape modelling	Ramesh	Fair results	Fair results	±
	Clustering-based	Iterative	Ridler	Very good results	Very good results	+
			Yanni	Good results	Good results	+
		Clustering	Otsu	Few details visible	Good results in dark regions	±
		Minimum error	Lloyd	Good results	Good results	+
			Kittler	Too few details	Too few details	−
		Fuzzy clustering	Jawahar_1	Too sensitive	Too sensitive	−
			Jawahar_2	Too sensitive	Too sensitive	−
	Entropy-based	Entropic	Kapur	Good results	Too dark	±
			Sahoo	Good results	Too light	±
			Pun_1	Too few details	Too few details	−
			Pun_2	Too few details	Too few details	−
		Cross entropic	Li	Good results	Too light	±
			Brink	Too few details	Too few details	−
		Fuzzy entropic	Shanbag	Too light	Too few details	−
	Object attribute-based	Moment preserving	Tsai	Good results	Good results	+
		Edge field matching	Hertz	Very good results	Very good results	+
		Fuzzy similarity	Huang	Too light	Fair results	±
			OGorman	Too light	Too few detais	−
		Topological stable-state	Pikaz	Good results	Too dark	−
	Spatial	Co-occurence	Pal_1	Too light	Too few details	−
			Pal_2	Too light	Too few details	−
		Higher-order entropy	Abutaleb	Very good results	Very good results	+
			Beghdadi	Too light	Too light	−
	Local	Variance	Niblack	Very good results	Bad results	−
			Sauvola	Good results	Bad results	−
		Contrast	White	Very bad results	Very bad results	−
			Bernsen	Bad results	Bad results	−
			Yasuda	Too angular	Too dark	−
		Center-surround scheme	Palumbo	Too abrupt/angular	Too abrupt/angular	−
			Kamel	Too light	Too light	−
		Surface-fitting	Yanowitz	Fair results	Few details visible	±

Abutaleb (Fig. 2f, j and l), given that these algorithms resulted in fair to excellent results in the centre and at the edges of the hemispherical images, in both sunlit and dark conditions.

3.2. Quantitative performance score

The AVE scores, based on the analysis of the selected 50 photographs, are presented in Table 5,

grouped per thresholding method category. Since AVE is an error score ranging from 0 to 1, the lower AVE (near 0), the better the performance of the algorithm, whereas the higher AVE (towards 1), the worse the performance.

According to the quantitative AVE scores, the 10 best methods were from the clustering, entropy, shape and attribute categories, which indicated the quantitative potential of these categories to binarization of hemispherical canopy images. However, given that the AVE is an average score based on five performance criteria, caution is somehow required since a method might have insufficient visual results and nevertheless a low AVE score (and vice versa). Fig. 3i illustrates

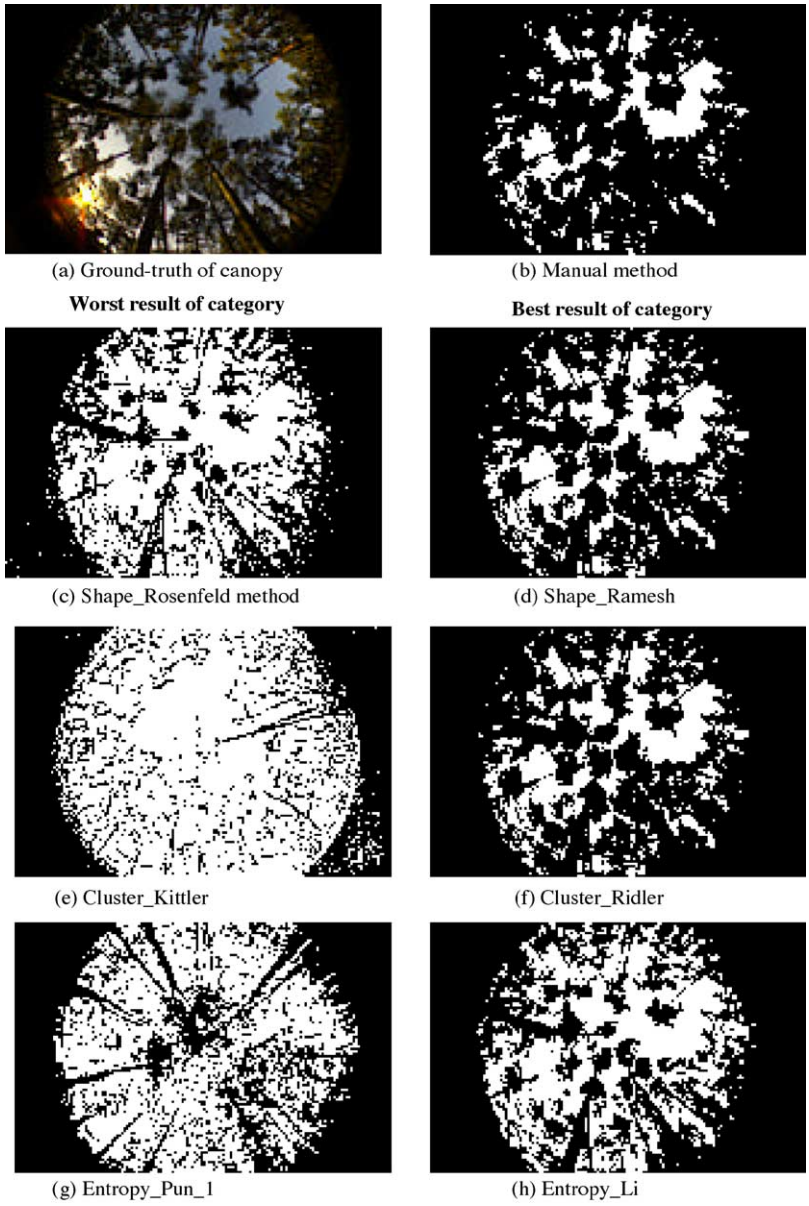

Fig. 2. Results of the worst and best thresholding algorithms for the six tested algorithm categories base on visual inspection, compared to the reference ground-truth hemispherical canopy image and manually thresholded image.

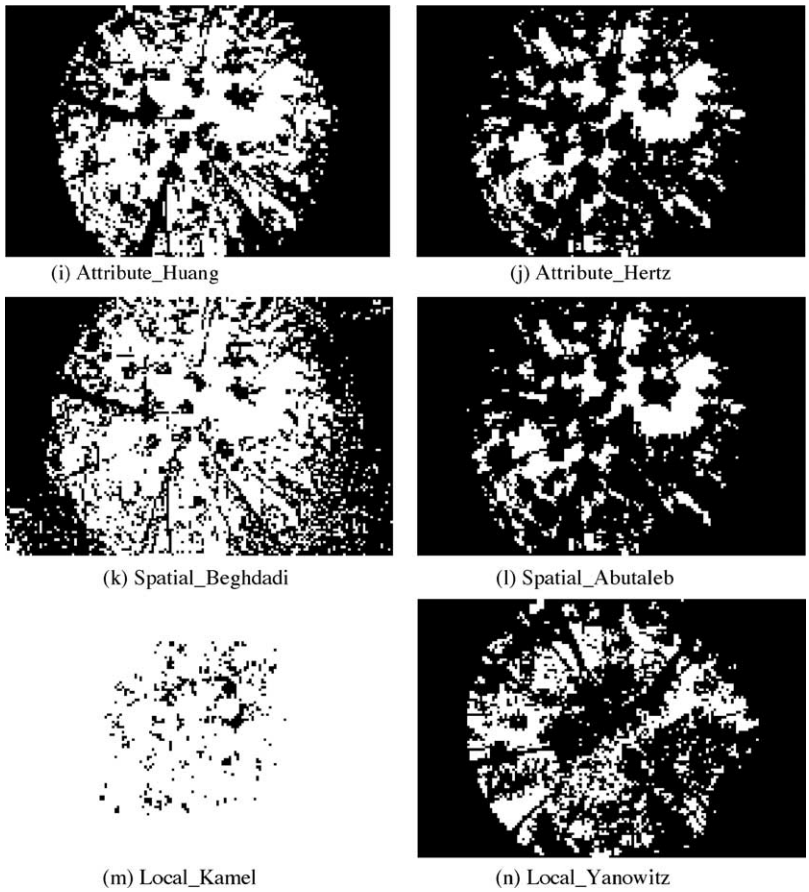

Fig. 2. (*Continued*).

this for the entropy-based Brink method, which had with the lowest performance AVE score of all thresholding methods tested (0.130, Table 5), but resulted in too few details for the purpose of gap fraction extraction. This demonstrates the need for both visual inspection and quantitative analysis of the photographs. The method with the best visual result and lowest AVE was consequently chosen for the selection of the optimal threshold. The iterative clustering method of Ridler was found to be the optimal method based on these criteria. This method yielded the best visual results for both coniferous and deciduous forest stands under different light conditions, and resulted in the lowest, thus best AVE score (0.174 ± 0.264) for the visual best methods. The small standard deviation indicated the robustness of the technique for different conditions (Fig. 2f and Table 5).

3.3. Optimal automatic thresholding method

The iterative Ridler clustering-based technique for thresholding calculates a global threshold (T) for the image based on clustering of the gray levels. The method initially segments the histogram of the color image into two parts using a starting threshold value of $T^0 = 2^{p-1}$, i.e. half the maximum dynamic range ($T^0 = 32{,}768$ in the case of 16-bit imagery). The sample mean ($m_{f,\,0}$) of the gray values associated with the foreground (vegetation) pixels and the sample mean ($m_{b,\,0}$) of the gray values associated with the background (sky) pixels are computed. A new threshold value (T^1) is then computed as the average of these two sample means. The process is repeated (k times), based upon the new threshold, until the threshold value remains constant. This

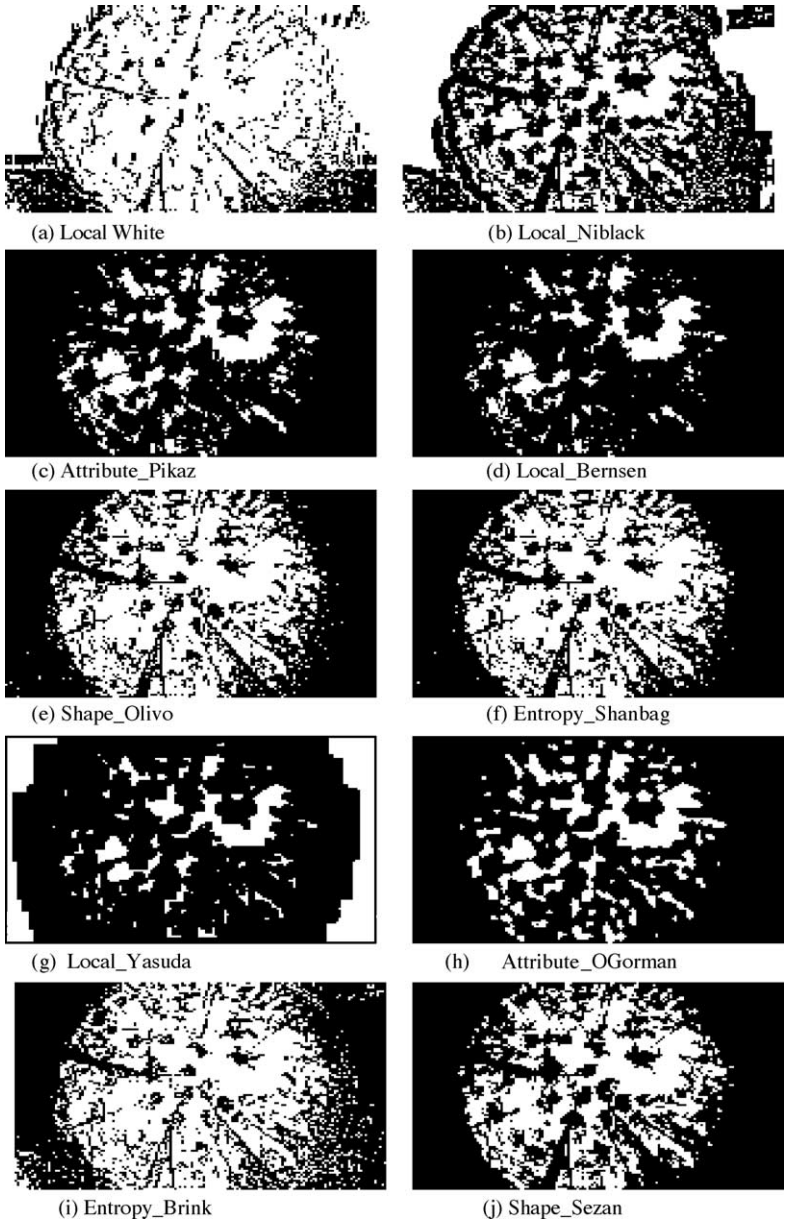

Fig. 3. Some particular thresholding problems based on visual inspection of the thresholded images.

final threshold is then used to binarize the image. The formula looks as follows (Ridler and Calvard, 1978):

$$T_{\text{opt}} = \lim \frac{(m_{\text{f},k-1} + m_{\text{b},k-1})}{2} \quad (3)$$

until

$$T^k = T^{k-1}$$

All digital hemispherical images used in the sensitivity analysis for gap fraction were automatically

Table 5
Thresholding evaluation ranking for all thresholding methods according to the overall average quality score AVE

	Category	Method	Mean average score	Standard deviation	Overall ranking
Manual		Fixed threshold = 110	0.1852	0.2813	18
Automatic	Histogram shape-based	Sezan	0.1400	0.2121	2
		Olivo	0.1486	0.2264	4
		Rosenfeld	0.1490	0.2271	5
		Ramesh	0.1808	0.2743	14
	Clustering-based	Ridler	0.1744	0.2638	9
		Otsu	0.1748	0.2644	10
		Jawahar_1	0.1750	0.2647	11
		Lloyd	0.1754	0.2653	12
		Yanni	0.1918	0.2902	19
		Jawahar_2	0.3652	0.5628	31
		Kittler	0.3652	0.5629	32
	Entropy-based	Brink	0.1301	0.1985	1
		Pun_1	0.1442	0.2185	3
		Li	0.1530	0.2314	7
		Sahoo	0.1828	0.2788	16
		Shanbag	0.2006	0.3128	21
		Kapur	0.2236	0.3581	25
		Pun_2	0.2758	0.4279	28
	Object attribute-based	Huang	0.1516	0.2294	6
		Tsai	0.1764	0.2670	13
		Hertz	0.1812	0.2747	15
		Pikaz	0.2556	0.4166	27
		OGorman	0.7092	1.0724	36
	Spatial	Pal_2	0.1540	0.2336	8
		Beghdadi	0.2084	0.3215	22
		Abutaleb	0.2158	0.3344	24
		Pal_1	0.2429	0.3907	26
	Local	Yanowitz	0.1844	0.2791	17
		Bernsen	0.2004	0.3047	20
		Palumbo	0.2124	0.3291	23
		Sauvola	0.2828	0.4587	29
		Niblack	0.3072	0.4648	30
		White	0.4294	0.6508	33
		Yasuda	0.4378	0.6628	34
		Kamel	0.5444	0.8274	35

AVE is based on five quantitative evaluation parameters (Sezgin and Sankur, 2004). The automatic methods are presented in groups according to the six respective thresholding categories.

converted to binary images by applying the Ridler clustering analysis script to the blue-filtered gray scale histogram of the photograph. This was done by means of an in-house developed IDL-script. All pixels that had a blue-layer grayscale intensity lower than the threshold determined by cluster analysis, were converted into black (1 = foliage), while all other pixels were converted into white (0 = sky). Fig. 4 shows selected examples of images thresholded both manually and by the automatic clustering method of Ridler.

3.4. Sensitivity analysis

3.4.1. Operator bias

The automatic thresholding method is an alternative for the traditional, manual method, which aside from its

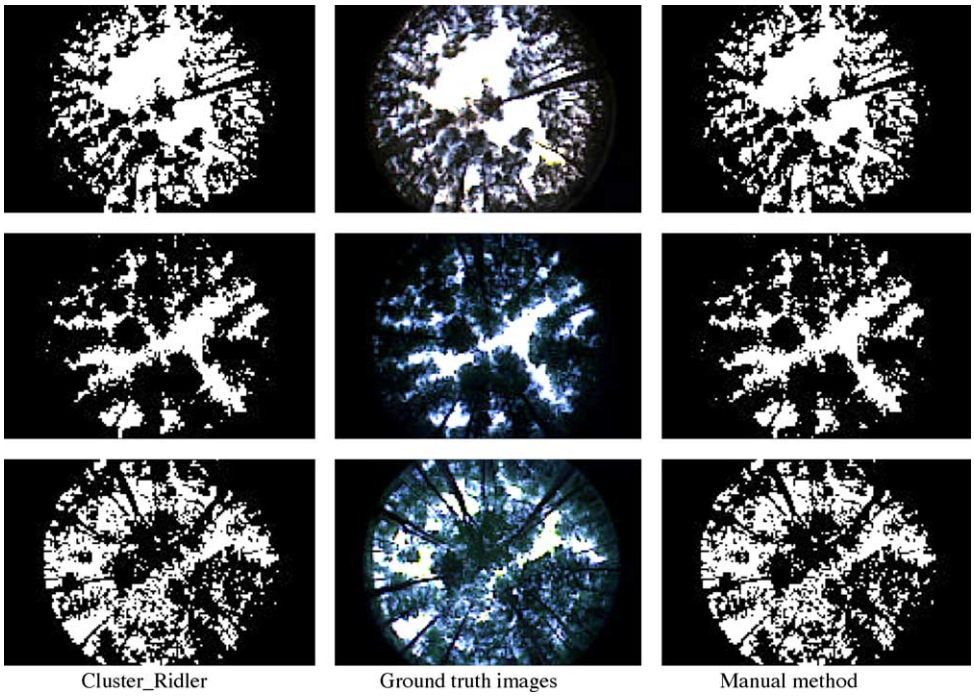

Fig. 4. Ground-truth images and respective Cluster–Ridler, and manual thresholding results. The photographs were taken in Pijnven on 7 October 2002, in Meerdaalwoud on 6 March 2002 and in Zoniënwoud on 10 October 2003, respectively.

time-consuming character has the disadvantage to be subject to variation caused by the operator. The thresholding needs some interpretation and experience from the operator for visual determination of a threshold value for converting a gray scale image to a binary image, which makes the results operator-dependent. The bias caused by the operator's subjectivity in the manual method was therefore investigated.

Ten experienced operators were asked to manually threshold 10 randomly selected hemispherical canopy photographs. Gap fraction was derived from these thresholded images and the results were compared (Fig. 5). Fig. 5 shows for each of the selected images the maximum, minimum and medium gap fraction, obtained from the binary images by the 10 different operators, compared to the result of the automatic

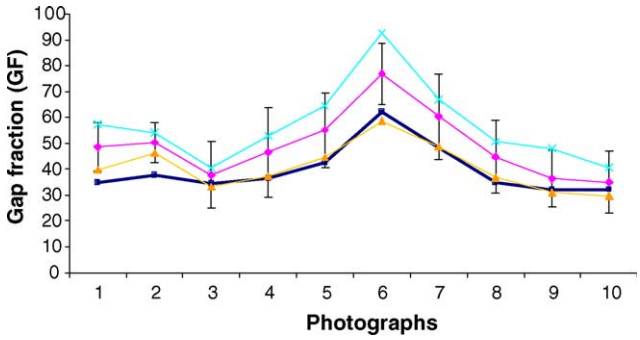

Fig. 5. Influence of operator on gap fraction. The automatic Ridler method (■) is presented with the, respectively, maximum (×), minimum (▲) and mean (◆) gap fraction (GF) values for the 10 manual thresholded images by 10 different operators. The whiskers represent the standard deviations of the mean.

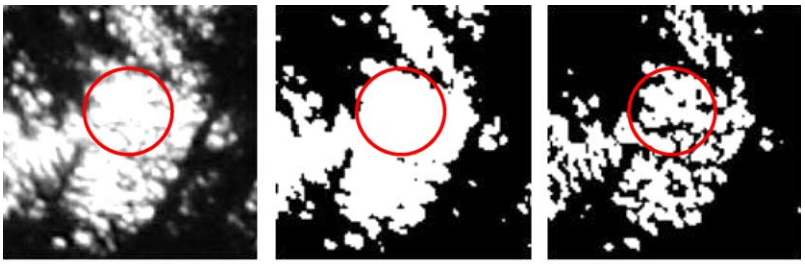

Fig. 6. Detailed analysis of ground-truth image, global Ridler, and Ridler combined with local Niblack thresholding results. The original photograph was taken in Pijnven on 7 October 2002.

Ridler method. The graph shows that variation becomes higher as the gap fraction of the image increases. A possible explanation for the higher GF values corresponding to manual thresholding is the fact that most operators focus on the edges of sky and foliage where distinction between foliage and sky is easiest to make. The selected threshold value is thus optimal solely for these regions, though not for the larger proportion of the image with more dense foliage and small gaps. However, more importantly, these results provide a unique insight into the reduction of variability in measured GF when using an automated thresholding method without a need for user interference. This experiment corroborated that the variation of the results, caused by the operator dependency provides an extra disturbing factor that interferes with reproducibility, and makes comparisons of different sites and studies less reliable.

3.4.2. *Uneven luminance conditions*

A global threshold was found the most robust technique for thresholding high-dynamic range hemispherical images for various camera settings and canopy structure conditions. Local thresholding, however, may be necessary in case the image is unevenly illuminated, since global techniques are not able to cope with the variation in received light intensities over the hemispherical image. Variable luminance in digital photographs may occur due to spatial variation of sky brightness or image brightness introduced by the hemispherical lens. In local thresholding, a threshold value is assigned to each pixel to determine whether it is a foreground or background pixel using local information from the image. We investigated, therefore, the potential to refine the optimal "global" Ridler method by means of a local method in case of luminance differences over the hemispherical image.

The example of local over-exposure in a hemispherical image was investigated by using a detail of a hemispherical image with more open area in the canopy, where sunlit foliage occurs due to scattering (Fig. 6). The vegetation pixels resulted classified as sky by means of the global Ridler method. In order to deal with this local over-exposure problem, a local method performing well in the lighter areas of the image is needed. As the visual inspection showed that the local method of Niblack performed well in light areas (Table 4), we tested this local method as correction for the sunlit area which was misclassified by the global Ridler method. We tested the combination of the local methods of Niblack and the global Ridler technique via a Boolean logic OR operation on both binary images in ENVI. This is illustrated in the detailed study (Fig. 6), where the pixels in the region of interest of the image, clearly belonging to sunlit foliage, are classified as vegetation cover by global Ridler combined with the local Niblack method, but seen as sky pixels by global Ridler method. Detailed visual inspection corroborated the statement that the combination of both global and local method made it possible to better address variable brightness in the image, which resulted in a better classification of the vegetation pixels in the sunlit region (Fig. 6).

4. Discussion

Automatic thresholding algorithms have been evaluated using digital hemispherical color photo-

graphs of forest canopies. The results of this thresholding step are very important as it has significant influence on the subsequent gap fraction determination. Under-thresholding is undesirable as it can lead to the loss of foliage, particularly where sunlit foliage is classified as sky. Conversely, the dangers of over-thresholding can be much more subtle and might even extend beyond over-estimation of the gap fraction. This has off course a major impact on the estimated gap fraction out of the hemispherical images.

The visual inspection of the photographs by means of multi-criteria analysis resulted in the identification of three well-performing algorithms: the Cluster–Ridler method, the object-attribute based method of Hertz, and the spatially based Abutaleb method. The good performance of the Ridler method is in agreement with Lievers and Pilkey (2004), who studied segmentation of automotive aluminium sheet alloys. However, no absolute comparison is possible, since the performance of thresholding algorithms are application-based and there are no known studies concerning the application of this algorithm in a forestry context.

The quantitative analysis resulted in a top 10 ranking of methods of the groups of cluster, shape-based, object attribute-based and entropy, which is in agreement with Sezgin and Sankur (2004). The authors ranked the categories of clustering and entropy highest, and thus most plausible for thresholding of non-destructive images. The clustering method of Ridler was considered the ''optimal'' automatic thresholding method for the binarization of hemispherical photographs, based on the combination of visual analysis and the performance analysis of the AVE values. The algorithm is able to produce accurate silhouettes for the extraction of gap fraction from the blue-layer images of tree canopies, and has been found to be the most robust automatic thresholding technique for the different stand types (deciduous/coniferous and open/closed). This technique, which gave satisfactory results at image edges and in the center, for both dark and sunlit conditions, performed better than the other algorithms in terms of robustness under varying conditions. The clustering method of Ridler also achieved the best overall calculated performance AVE value. Some methods did perform well under specific sky conditions (sunlit or dark), but yielded unacceptable results under the opposite condition. The clustering Otsu and local Niblack method are examples of this, and performed well in, respectively, dark/sunlit regions, but were unable to distinguish foliage from sky in overly light/dark conditions. Local thresholding techniques were found to be inappropriate for application at photo-level. This was due to too little detail visible in the image centre and at the edges, which caused a substantial over-estimation of the gap fraction and consequently a significant under-estimation of LAI. This poor performance was attributed to the high level of complexity of such photographs.

The automatic methods also were very time-efficient, whereas interactive thresholding was very time-consuming. This suggests that, apart from the potential to provide an objective measure for canopy structure and light measurement, automatic thresholding allows considerably faster image processing.

In case of variable brightness over the hemispherical image, the combination of the local Niblack method with the Ridler method gave a superior performance over the existing optimal global Ridler thresholding technique, as the local method was able to cope with local over-exposure. More information should be used to assist the thresholding, and thus greater accuracy and more consistent performance is required in order to correct for these technical problems.

5. Concluding remarks

The global clustering method of Ridler was found to be the optimal and most robust automatic thresholding method for a wide range of light and canopy structure conditions. This automatic method was most robust in terms of both visual and quantitative analyses and provides a useful baseline against which more advanced algorithms can be evaluated. It therefore offers an alternative towards a fast, reliable and objective use of hemispherical photographs for gap fraction and LAI estimation in forest stands. A high level of accuracy and reproducibility is maintained, since the impact of the operator on the thresholding of high-dynamic range images revealed a considerable variation in gap fraction results. This variation does not occur when using automatic methods, which provides the advantage of repeatability and reliability

to compare different studies and sites in a more objective manner.

However, attention must be paid to the possible potential of fine-tuning of local thresholding methods to better address particular photographic limitations (e.g. over-exposure in a certain image region). The main scope of this study has been to find an alternative to the subjective manual thresholding method, and therefore enables further research to be done in order to address particular photographic problems. The use of new or more complex algorithms (tri- or multi-level thresholding) also might be tested, together with an investigation into the influence of image smoothing for noise elimination. Since ''real'' gap fraction cannot be explicitly measured, this evaluation has only a relative and not an absolute value. This issue can be addressed in the future by simulating virtual forest stands with known gap fractions, from which the optimal selected method can be validated by means of virtual hemispherical photographs.

Acknowledgements

We would like to thank Sigma Corporation (Tokyo, Japan) for providing us with data on the lens distortion for the Sigma 8 mm f/4 'fisheye' lens, used in the study. We would like to acknowledge the useful comments and criticisms about thresholding provided by Dr. Mehmet Sezgin (Tübýtak Marmara Research Centre, Gebze, Kocaeli, Turkey). The valuable editing by Dr. Jan Van Aardt also is deeply appreciated. Funding support for this research has been provided by FWO Flanders (Project no. G.0085.01).

References

Abutaleb, A.S., 1989. Automatic thresholding of gray-level pictures using two-dimensional entropy. Comput. Vision Graph. Image Proc. 47, 22–32.

Ackerly, D.D., Bazzaz, F.A., 1995. Seedling crown orientation and interception of diffuse radiation in tropical forest gaps. Ecology 76, 1134–1146.

Battaglia, M.A., Mou, P., Palik, B., Mitchell, R.J., 2002. The effect of spatially variable overstory on the understory light environment of an open-canopied longleaf pine forest. Can. J. Forest Res. 32, 1984–1991.

Blennow, K., 1995. Sky view factors from high-resolution scanned fish-eye lens photographic negatives. J. Atmos. Ocean. Tech. 12, 1357–1362.

Bockaert, V., 2004. The 123 of Digital Imaging Interactive Learning Suite, Version 3.0, p. 2780 (CD).

Chason, J.W., Baldocchi, D.D., Huston, M.A., 1991. A comparison of direct and indirect methods for estimating forest canopy leaf-area. Agric. Forest Meteorol. 57, 107–128.

Chen, J.M., 1996. Optically-based methods for measuring seasonal variation of leaf area index in boreal conifer stands. Agric. Forest Meteorol. 80, 135–163.

Chen, J.M., Black, T.A., Adams, R.S., 1991. Evaluation of hemispherical photography for determining plant area index and geometry of a forest stand. Agric. Forest Meteorol. 56, 129–143.

Englund, S.R., O'Brien, J.J., Clark, D.B., 2000. Evaluation of digital and film hemispherical photography for predicting understorey light in a Bornean tropical rain forest. Agric. Forest Meteorol. 97, 129–139.

ENVI, 2004. Information available from, http://www.rsinc.com/envi/.

Fernandes, R., Miller, J.R., Chen, J.M., Rubinstein, I.G., 2003. Evaluating image-based estimates of leaf area index in boreal conifer stands over a range of scales using high-resolution CASI imagery. Remote Sens. Environ. 89, 200–216.

Fraser, C.S., 1997. Digital camera self-calibration. Photogramm. Eng. Remote Sens. 52, 149–159.

Frazer, G.W., Trofymow, J.A., Lertzman, K.P., 1997. A method for estimating canopy openness, effective leaf area index, and photo synthetically active photon flux density using hemispherical photography and computerized image analysis techniques. K.P. Nat. Res. Canada, Can. For. Serv. Pacific For. Cent. Inf. Re BC-X-373, 75 p.

Frazer, G.W., Fournier, R.A., Trofymow, J.A., Hall, R.J.A., 2001. Comparison of digital and film fisheye photography for analysis of forest canopy structure and gap light transmission. Agric. Forest Meteorol. 109, 249–263.

Hale, S.E., Edwards, C., 2002. Comparison of film and digital hemispherical photography across a wide range of canopy densities. Agric. Forest Meteorol. 112, 51–56.

Herbert, T.J., 1986. Calibration of fisheye lenses by inversion of area projections. Appl. Opt. 25, 1875–1876.

Hinz, A., Dörstel, C., Heier, H., 2001. DMC2001-The Z/I imaging digital camera system. In: Proceedings of ASPRS Conference: Gateway to the New Millennium, 23–27 April, St. Louis, Missouri, USA, p. 3.

IDL, 2004. Information available from, http://www.rsinc.com/idl/.

ImageMagick, 2004. Information available from, www.imagemagick.org.

Jacquemoud, S., Baret, F., 1990. Prospect—a model of leaf optical-properties spectra. Remote Sens. Environ. 34, 75–91.

Jonckheere, I., Fleck, S., Nackaerts, K., Muys, B., Coppin, P., Weiss, M., Baret, F., 2004. Review of methods for in situ leaf area index determination. Part I. theories, sensors and hemispherical photography. Agric. Forest Meteorol. 121, 19–35.

Jonckheere, I., Muys, B., Coppin, P., 2005. Allometry and evaluation of in-situ optical LAI determination: a case-study in Belgium. Tree Physiol. 25 (6), 723–732.

Kapur, J., Sahoo, P., Wong, A., 1985. A new method for gray-level picture thresholding using the netropy of the histogram. Comput. Vision Graph. Image Proc. 29, 273–285.

Koller, D., Weber, J., Malik, J., 1994. Robust multiple car tracking with occlusion reasoning. In: European Conference of Computer Vision. pp. 189–196.

Kucharik, C.J., Norman, J.M., Murdock, L.M., Gower, S.T., 1997. Characterizing canopy non-randomness with a multiband vegetation imager (MVI). J. Geophys. Res. 102, 29455–29473.

Lievers, W.B., Pilkey, A.K., 2004. An evaluation of global thresholding techniques for the automatic image segmentation of automotive aluminium sheet alloys. Mater. Sci. Eng. 381, 134–142.

Mussche, S., Samson, R., Nachtergale, L., De Schrijver, A., Lemeur, R., Lust, N.A., 2001. Comparison of optical and direct methods for monitoring the seasonal dynamics of leaf area index in deciduous forests. Silva Fenn. 35, 373–384.

Nackaerts, K., Sterckx, S., Coppin, P., 1999a. Fractal dimension as correction factor for stand-level indirect leaf area index measurements. In: Proceedings of EOS/SPIE Symposium on Remote Sensing: Remote Sensing for Agriculture, Ecosystems, and Hydrology III, 20–24 September, Florence, Italy, pp. 80–89.

Nackaerts, K., Wagendorp, T., Coppin, P., Muys, B., Gombeer, R., 1999b. A correction of indirect LAI measurements for a non-random distribution of needles on shoots. In: Proceedings of ISSSR: Systems and Sensors for the New Millennium, October 31–4 November, Las Vegas, Nevada, USA, pp. 413–424.

Niblack, W., 1986. An Introduction to Image Processing. Prentice-Hall, Englewood Cliffs, NJ, pp. 115–116.

Oker-Blom, P., Kellomäki, S., 1983. Effect of grouping of foliage on the within-stand and within-crown light regime: comparison of random and grouping canopy models. Agric. Forest Meteorol. 28, 143–155.

Oker-Blom, P., Kaufmann, M.R., Ryan, M.G., 1991. Performance of a canopy light interception model for conifer shoots, trees and stands. Tree Physiol. 9, 227–243.

Olivo, J.C., 1994. Automatic threshold selection using the wavelet transform. Graph. Models Image Process 56, 205–218.

Otsu, N., 1979. A threshold selection method from gray level histograms. IEEE Trans. Syst. Man. Cybern. SMC 9, 62–66.

Ozanne, C.M.P., Anhuf, D., Boulter, S.L., Keller, M., Kitching, R.L., Korner, C., Meinzer, F.C., Mitchell, A.W., Nakashizuka, T., Dias, P.L.S., Stork, N.E., Wright, S.J., Yoshimura, M., 2003. Biodiversity meets the atmosphere: a global view of forest canopies. Science 301, 183–186.

PHP, 2004. Information available from, www.php.org.

Prewitt, J.M.S., Mendelsohn, M.L., 1966. The analysis of cell images. Ann. Acad. Sci. 128, 1035–1053.

Rhoads, A.G., Hamburg, S.P., Fahey, T.J., Siccama, T.G., Kobe, R., 2004. Comparing direct and indirect methods of assessing canopy structure in a northern hardwood forest. Can. J. Forest Res. 34, 584–591.

Rich, P.M., 1990. Characterizing plant canopies with hemispherical photographs. Remote Sens. Rev. 5, 13–29.

Rich, P.M., Clark, D.B., Clark, D.A., Oberbauer, S.F., 1993. Long-term study of solar radiation regimes in a tropical wet forest using quantum sensors and hemispherical photography. Agric. Forest Meteorol. 65, 107–127.

Ridler, W., Calvard, S., 1978. Picture thresholding using an iterative selection method. IEEE Trans. Syst. Man. Cyber. SMC 8, 260–263.

Rosin, P.L., Ioannidis, E., 2003. Evaluation of global image thresholding for change detection. Pattern Recognit. Lett. 24, 2345–2356.

Russ, J., 2002. The Image Processing Handbook, fourth ed. CRC Press, Florida, USA, p. 732.

Sezgin, M., Sankur, B., 2004. Survey over image thresholding techniques and quantitative performance evaluation. J. Electron. Imag. 13, 146–165.

Stenberg, P., Nilson, T., Smolander, H., Voipio, P., 2003. Gap fraction based estimation of LAI in Scots pine stands subjected to experimental removal of branches and stems. Can. J. Remote Sens. 29, 363–370.

ter Steege, H., 1997. WINPHOT, a Windows 3.1 Programme to Analyse Vegetation Indices, Light and Light Quality from Hemispherical Photographs. Tropenbos-Guyana Reports 97-3. Tropenbos-Guyana Programme, Georgetown, Guyana.

Tsai, W., 1985. Moment-preserving thresholding. Comput. Vision Graph. Image Proc. 29, 377–393.

Walter, J.M., Fournier, R.A., Soudani, K., Meyer, E., 2003. Integrating clumping effects in forest canopy structure: an assessment through hemispherical photographs. Can J. Remote Sens. 29, 388–410.

Watson, D.J., 1947. Comparative physiological studies in growth of field crops. I. Variation in net assimilation rate and leaf area between species and varieties, and within and between years. Ann. Bot. 11, 41–76.

Weiss, M., 2003. EYE-CAN, Version 1.4, unpublished software documentation. INRA, CSE/Noveltis, Avignon, France.

Weiss, M., Baret, F., Smith, G., Jonckheere, I., Coppin, P., 2004. Review of methods for in situ leaf area index determination, Part II. Estimation of LAI, errors and sampling. Agric. Forest Meteorol. 121, 37–53.

Xite, 2004. Information available from, http://www.ifi.uio.no/forskning/grupper/dsb/Programvare/Xite/.

Zar, J.H., 1984. Biostatistical Analysis, second ed. Prentice Hall Inc., NJ, USA, p. 361.